

JWST AND ALMA IMAGING OF DUST-OBSCURED, MASSIVE SUBSTRUCTURES IN A TYPICAL $z \sim 3$ STAR-FORMING DISK GALAXY

WIPHU RUJOPAKARN^{1,2}, CHRISTINA C. WILLIAMS^{3,4}, EMANUELE DADDI⁵, MALTE SCHRAMM⁶, FENGWU SUN⁴, STACEY ALBERTS⁴, GEORGE H. RIEKE⁴, QING-HUA TAN (谈清华)⁷, SANDRO TACCHHELLA^{8,9}, MAURO GIAVALISCO¹⁰, AND JOHN D. SILVERMAN¹¹

¹National Astronomical Research Institute of Thailand, Don Kaeo, Mae Rim, Chiang Mai 50180, Thailand; wiphu@narit.or.th

²Department of Physics, Faculty of Science, Chulalongkorn University, 254 Phayathai Road, Pathumwan, Bangkok 10330, Thailand

³NSF's National Optical-Infrared Astronomy Research Laboratory, 950 North Cherry Avenue, Tucson, AZ 85719, USA

⁴Steward Observatory, The University of Arizona, Tucson, AZ 85721, USA

⁵Université Paris-Saclay, Université Paris Cité, CEA, CNRS, AIM, 91191, Gif-sur-Yvette, France

⁶Universität Potsdam, Karl-Liebknecht-Str. 24/25, D-14476 Potsdam, Germany

⁷Purple Mountain Observatory, Chinese Academy of Sciences, 10 Yuanhua Road, Nanjing 210023, People's Republic of China

⁸Kavli Institute for Cosmology, University of Cambridge, Madingley Road, Cambridge, CB3 0HA, UK

⁹Cavendish Laboratory, University of Cambridge, 19 JJ Thomson Avenue, Cambridge, CB3 0HE, UK

¹⁰Department of Astronomy, University of Massachusetts, B 619E 710 North Pleasant Street Amherst, MA, USA

¹¹Kavli IPMU (WPI), UTIAS, The University of Tokyo, Kashiwa, Chiba 277-8583, Japan

Draft version April 11, 2023

ABSTRACT

We present an identification of dust-attenuated star-forming galactic-disk substructures in a typical star-forming galaxy (SFG), UDF2, at $z = 2.696$. To date, substructures containing significant buildup of stellar mass and actively forming stars have yet to be found in typical (i.e., main-sequence) SFGs at $z > 2$. This is due to the strong dust attenuation common in massive galaxies at the epoch and the scarcity of high-resolution, high-sensitivity extinction-independent imaging. To search for disk substructures, we subtracted the central stellar-mass disk from the *JWST*/NIRCam rest-frame 1.2 μm image ($0''.13$ resolution) and subtracted, in the visibility plane, the central starburst disk from ALMA rest-frame 240 μm observations ($0''.03$ resolution). The residual images revealed substructures at rest-frame 1.2 μm co-located with those found at rest-frame 240 μm , $\simeq 2$ kpc away from the galactic center. The largest substructure contains $\simeq 20\%$ of the total stellar mass and $\simeq 5\%$ of the total SFR of the galaxy. While UDF2 exhibits a kinematically-ordered velocity field of molecular gas consistent with a secularly evolving disk, more sensitive observations are required to characterize the nature and the origin of this substructure (spiral arms, minor merger, or other types of disk instabilities). UDF2 resides in an overdense region ($N \geq 4$ massive galaxies within 70 kpc projected distance at $z = 2.690 - 2.697$) and the substructures may be associated with interaction-induced instabilities. Importantly, a statistical sample of such substructures identified with *JWST* and ALMA could play a key role in bridging the gap between the bulge-forming starburst and the rest of the galaxy.

Subject headings: galaxies: evolution — galaxies: structure

1. INTRODUCTION

The groundbreaking angular resolution and sensitivity of far-IR/submillimeter (submm) observations from the Atacama Large Millimeter/submillimeter Array (ALMA) and the subsequent flurry of blank-field interferometric submm surveys have enabled capturing an unbiased sample of *typical*¹ star-forming galaxies (SFGs) at $z \sim 1 - 4$ that represents the assembly sites of most stellar mass in the Universe independent of their dust attenuation (e.g., Dunlop et al. 2017; Elbaz et al. 2018).

Sub-arcsecond ALMA observations of typical SFGs at this epoch have revealed a common pattern: they contain a compact region of intense star formation (SF) at their centers. These central star-forming regions usually harbor star-formation rate (SFR) of $\sim 100 - 300 M_{\odot} \text{yr}^{-1}$ within $r_{\text{SF}} \sim 0.5 - 1$ kpc, which is $\sim 2 - 5$ times more

compact than the extent of their stellar buildups virtually independently of the way they are selected, e.g., far-IR/submm blank field surveys (Dunlop et al. 2017; Fujimoto et al. 2018; Elbaz et al. 2018), H α -selected galaxies (Tadaki et al. 2017), or optically-selected massive compact SFGs (Barro et al. 2016).

Zooming in further, high-S/N sub- $0''.1$ ALMA observations that can confirm or rule out substructures of SF are still scarce, but early results indicate that these central star-forming regions are strikingly smooth (Rujopakarn et al. 2019; Ivison et al. 2020). There has been no identification of off-center structures containing significant SFR in typical SFGs thus far — ALMA identification of SF substructures at $z > 2$ so far are in luminous submm-selected galaxies (e.g., Swinbank et al. 2015; Iono et al. 2016; Tadaki et al. 2018; Hodge et al. 2019). Also, the UV-bright clumps commonly found in typical SFGs at $z \gtrsim 1$ contain $\lesssim 1\%$ of the total SF and molecular gas. That is, the UV-bright clumps are not the signposts for the ‘tip of the iceberg’ beneath which the bulk of SF is occurring (Cibinel et al. 2017; Rujopakarn et al. 2019).

For typical SFGs at $z > 2$, the connection between

¹ Typical star-forming galaxies are defined here as those with SFR within a factor of four of the main-sequence (e.g., Rodighiero et al. 2011) at their corresponding redshift on all of the following main-sequence parameterizations: Whitaker et al. (2012); Speagle et al. (2014), and Schreiber et al. (2015), hereafter ‘typical SFGs’.

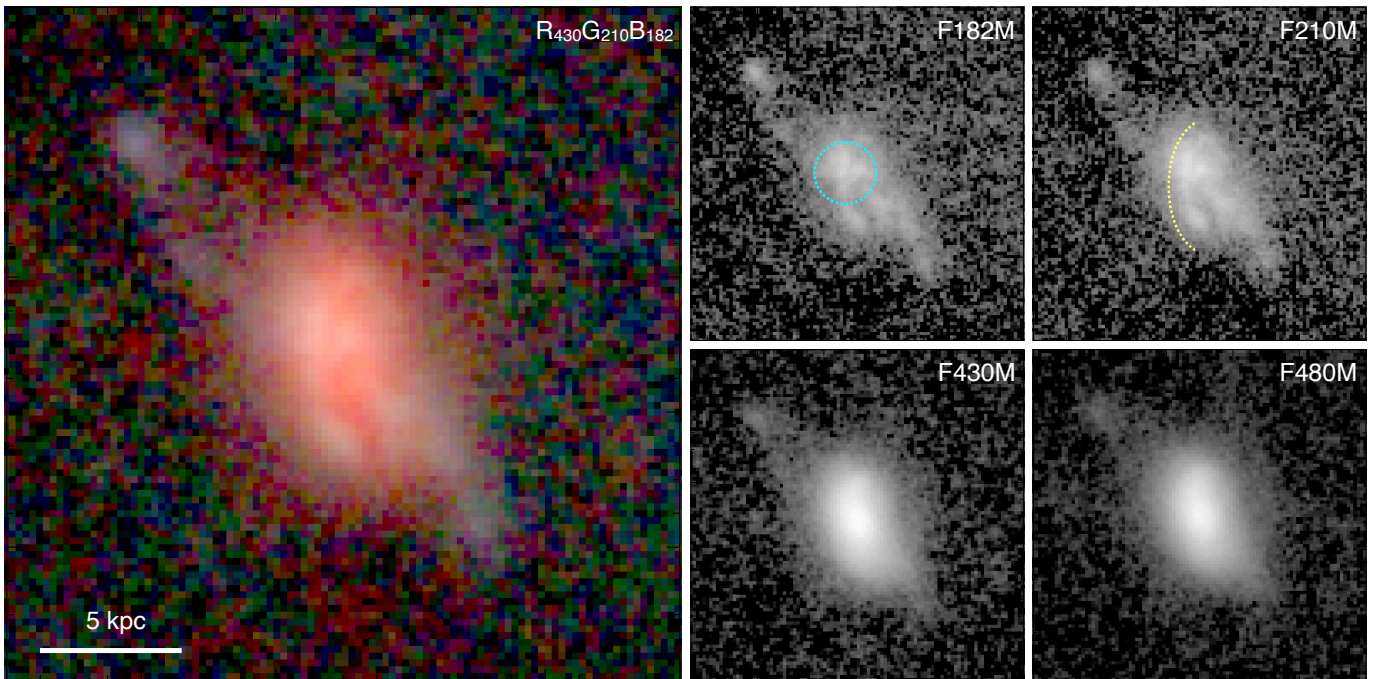


FIG. 1.— *JWST* images of UDF2. The left panel shows *JWST* color composite; the four sub-panels on the right show F182M image with the cyan dotted circle indicating the position of the brightest feature previously seen in *HST*/F160W image (Figure 1 of Rujopakarn et al. 2019) that is now resolved into multiple point-like features; F210M image with the yellow dotted arc indicating the semicircular feature around the center of stellar mass distribution that is clearly visible in the F430M and F480M images. Each cutout is $3'' \times 3''$; north is up, east is to the left.

their compact core observed at far-IR/submm and their extended optical morphologies remains unclear. Bridging this gap requires finding off-center substructures that are detected in *both* far-IR/submm and optical bands, which represent the sites of SF and stellar mass buildups, respectively. Identification of off-center substructures with substantial presence of stellar mass and harboring significant SFR could indicate, e.g., spiral arms or other types of disk instability. Notably, rest-frame optical images of typical SFGs often exhibit strong dust attenuation in the proximity of the far-IR/submm emission (Nelson et al. 2019; Rujopakarn et al. 2016, 2019), which suggest that *JWST* observations will play a key role in bridging the gap between optical and far-IR/submm pictures.

In this Letter, we report the first identification of off-center massive substructures in a typical SFG at $z \sim 3$ that is detected in both *JWST*/NIRCam and ALMA observations. We adopt a Λ CDM cosmology with $\Omega_M = 0.3$, $\Omega_\Lambda = 0.7$, $H_0 = 70 \text{ km s}^{-1} \text{ Mpc}^{-1}$, where $1''$ at $z = 2.7$ corresponds to 7.9 kpc, and the Salpeter IMF.

2. TARGET AND OBSERVATIONS

Our target (“UDF2”) was identified as a main-sequence SFG via an ALMA blank-field survey (Dunlop et al. 2017) of the Hubble Ultra Deep Field (HUDF). It has a total SFR of $260 M_\odot \text{ yr}^{-1}$ and $\log(M_*/M_\odot) = 10.9 \pm 0.2$ (Rujopakarn et al. 2019) at $z = 2.6961$ (Kaasinen et al. 2020). *HST* imaging of UDF2 at $0.6\text{--}1.6 \mu\text{m}$ (rest-frame $0.2\text{--}0.4 \mu\text{m}$) show disturbed morphology extending up to $2''.5$ ($\simeq 20 \text{ kpc}$) whereas the dust emission observed by ALMA originates from within the central 3 kpc region (Rujopakarn et al. 2016).

UDF2 is a subject of a sensitive search for SF substructure employing ALMA rest-frame $240 \mu\text{m}$ dust continuum observations at $42 \times 30 \text{ mas}$ resolution and 9.6

$\mu\text{Jy beam}^{-1}$ rms sensitivity (Rujopakarn et al. 2019), which finds that the cold dust is distributed in a smooth disk with no substructures at the 200 pc scale. This data set remains one of the highest angular resolution imaging at the highest S/N of a typical SFG at $z > 2$ to date.

Kaasinen et al. (2020) further revealed by means of CO(3–2) observations at $0''.88 \times 0''.61$ resolution that this disk is kinematically-ordered, well-described by a single rotating component with maximum rotational velocity, $V_{\text{rot,max}} = 349_{-23}^{+19} \text{ km s}^{-1}$ and velocity dispersion, $\sigma = 77_{-11}^{+10} \text{ km s}^{-1}$. The corresponding V/σ ratio of 4.5 ± 0.7 is considerably more ‘dynamically cold’ than disk galaxies at its epoch (cf. compilation by Rizzo et al. 2020). While a kinematically-ordered velocity field does not necessarily preclude mergers (e.g., Simons et al. 2019), these observations lend credence to a picture of UDF2 being an isolated rotating disk, representative of typical SFGs at $z \sim 3$.

UDF2 was observed with *JWST*/NIRCam as a part of the *JWST* Extragalactic Medium-band Survey (JEMS; Program ID: 1963; PI: Williams). Observations were taken on 2022 October 11 in five filters, namely F182M, F210M, F430M, F460M, and F480M. The integration time was 28 ks in each filter (except F430M and F460M which were 14 ks each). The data reduction process is described in detail in Williams et al. (2023). The final mosaics are sensitive to 29.3, 29.2, 28.5, 28.3, and 28.6 AB mag (5σ , point source) in the ascending order of wavelength and are resampled to 30 mas pixel size. We independently inspect the astrometry of the final mosaic with 30-mas ALMA images of the nearby UDF1, 3, and 7 (whose astrometry is tied to the ICRF to $\simeq 2 \text{ mas}$; Rujopakarn et al. 2019) and find that the offsets between brightest features in ALMA and *JWST*

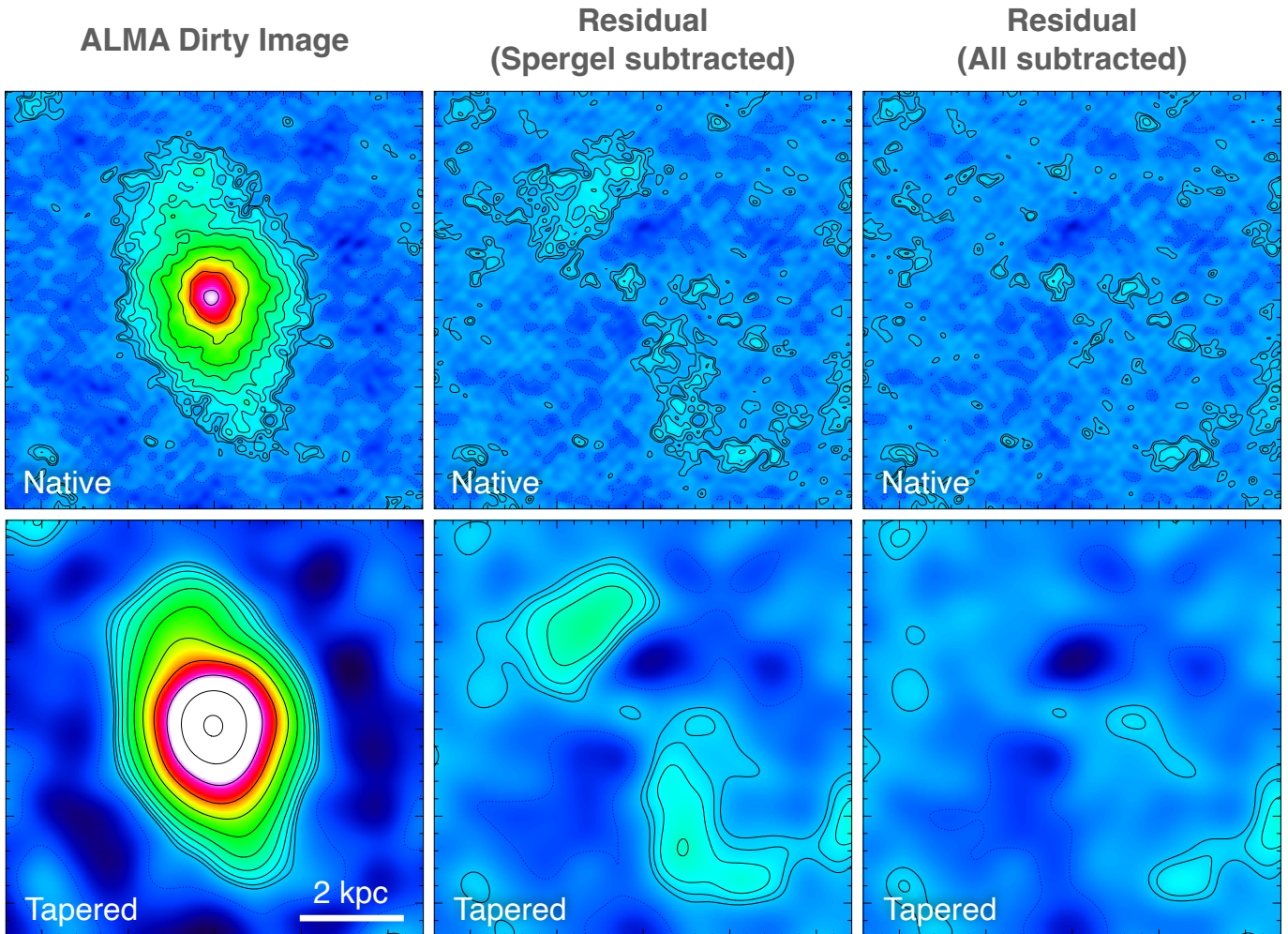


FIG. 2.— To search for substructures in UDF2’s star-forming regions, we subtract from the ALMA rest-frame $240\ \mu\text{m}$ continuum visibilities a Spergel profile (an approximation of the Sérsic profile with analytical Fourier transform). From left to right is the dirty ALMA image, the residual map with the main dust disk modeled by a single Spergel profile subtracted, and the residual after all components are subtracted, respectively. The top row is the native resolution image, whereas the bottom row is tapered at 1000 meters to enhance the sensitivity to extended features. Each cutout is $1'' \times 1''$; north is up, east is to the left; contours are $[-1.5, 1.5, 1.5^{1.5}, 1.5^2, \dots] \times \sigma$.

images are sub-pixel (i.e., < 30 mas).

3. IDENTIFICATION OF GALACTIC-DISK SUBSTRUCTURES

To search for galactic-disk substructures, we model and subtract the central component from ALMA and *JWST* images to search for co-locating residuals in both bands. We note that the galaxy ‘center’ refers to the centroid of the dust emission from the ALMA observations, whose position is localized within $\simeq 2$ mas.

3.1. Rest-frame optical/near-IR morphology from *JWST*

The *JWST* images of UDF2 are shown in Figure 1. The most striking feature is the presence of a single stellar mass component, seen in all long-wavelength filters (F430M-F480M; rest-frame $1.2 - 1.3\ \mu\text{m}$), but not obvious at shorter wavelength bands. The long-wavelength images show an isolated disk with no major morphological disturbance. This represents the true stellar mass distribution, an observation that was not previously measurable in *HST*/F160W image because of the dust attenuation. The centroid and position angle of the stellar mass component is in close alignment with that of the

cold dust disk and the rotation plane of the molecular gas disk (Figure 7 of Kaasinen et al. 2020).

The F182M and F210M images (rest-frame $0.5 - 0.6\ \mu\text{m}$) show a more complex morphology including clumpy substructures surrounding the location of the stellar mass buildup. The F182M image contains a bright region $0''.2$ northeast of the center, which corresponds to a prominent point-like feature in *HST*/F160W image (owing to the lower resolution). This bright region becomes less pronounced in F210M, where it appears to be a part of a semicircular feature (yellow arc in Figure 1) surrounding the location of the stellar mass buildup.

3.2. Identification of star-forming substructures

To search for off-center cold dust substructures that could indicate galactic-disk SF, we re-analyze the ALMA rest-frame $240\ \mu\text{m}$ observations of UDF2 using the visibility-based modeling technique described in Rujopakarn et al. (2019). In the previous analysis, we modeled the SF disk using superpositioned Gaussians to represent the Sérsic profile (Hogg & Lang 2013) because the latter lacks the analytical Fourier transform necessary for the visibility-based analysis. The best fit model was

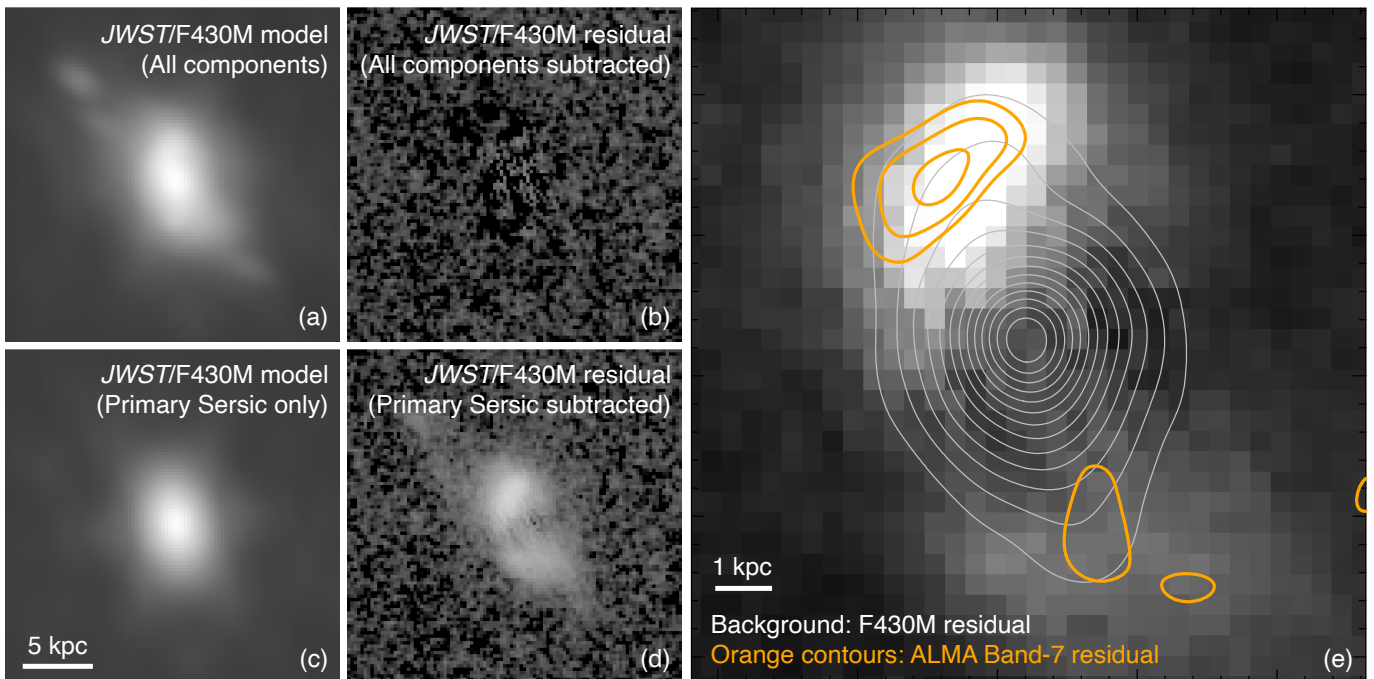


FIG. 3.— To search for substructures in the stellar mass distribution, we first model all components of the F430M emission (a), whose subtraction from the original image affords a flat residual (b), then only subtract the Primary Sérsic model of the stellar mass disk (c). The residuals in (d) indicate the presence of stellar mass substructures northeast and southwest of the galaxy center. Cutouts in panels (a) to (d) are $3'' \times 3''$ and with a log scaling. Panel (e) shows the central $1'' \times 1''$ of the residuals in panel (d) with a linear scaling; the tapered ALMA residuals overplotted as orange contours starting from 3σ in 1σ increment. The grey contours show the pre-subtraction ALMA continuum, tapered to the same scale, starting from 3σ in 5σ increment. The substructure in the northeast harboring SF and significant stellar mass buildup, dubbed the “northern ridge” is clearly visible.

a double concentric Gaussian that affords an approximation of a Sérsic. A region approximately $0''.2$ northeast of the center contains some residual flux peaking at $\simeq 2.9\sigma$, though the lack of definitively associable *HST* counterpart at its position (see Figures 1 and 2 of Rujopakarn et al. 2019) precludes the recognition of its significance over other sub- 3σ noise peaks.

In this analysis, we employ the newly implemented Spergel (2010) profile in GILDAS version nov22a, which offers an accurate representation of the Sérsic profile without relying on multiple components and featuring an analytical Fourier transform. The Spergel profile is characterized by the Spergel index ν , flux, and half-light radius (Spergel 2010), where Spergel ν plays a similar role to the Sérsic n . Within a range of ν , the Spergel profiles resemble Sérsic profiles. For example, at $\nu = 0.5$, the Spergel profile is identical to an exponential profile ($n = 1$). The robustness of the GILDAS implementation of Spergel fitting was tested using simulations by Kalita et al. (2022); a robust mapping between the Sérsic n and Spergel ν will be presented in Q. Tan et al., in prep.

We fit all three galaxies in the ALMA beam (UDF1, 2, and 7) using the Spergel profile simultaneously using the GILDAS `uv_fit` task. The best-fit Spergel profile of UDF2 has major and minor axes of 135 ± 3 mas and 65 ± 2 mas, respectively, $\nu = -0.28 \pm 0.04$, and a flux of $2885 \pm 106 \mu\text{Jy}$. After subtracting the best-fit Spergel profile in the uv -plane, two regions of residual remain: one at the northeast and southwest of the galaxy center (Figure 2). The northeast one, in particular, peaks at 5.5σ when Gaussian tapering is applied to baselines longer than 1000 meter (which results in a synthesized beam of $0''.16 \times 0''.13$ — similar to that of

JWST/F430M). We measure the fluxes of these substructures by fitting — in the uv -plane — elliptical Gaussians centering at the peaks of the substructure in the tapered image. The residual maps after subtracting the best-fit models, from which we have measured the substructure fluxes are shown in the ‘All subtracted’ column in Figure 2. The total flux in the northeast and southwest substructures are 172 ± 28 and $148 \pm 42 \mu\text{Jy}$, respectively, each being $\simeq 5\%$ of the total flux of the entire galaxy.

3.3. Identification of stellar-mass substructures

To search for off-center stellar mass buildups that serve as a proxy for galactic disk substructures, we perform a GALFIT decomposition on the F430M image by modeling the source following the same procedure performed on the *HST* images in Rujopakarn et al. (2019). The F430M image is chosen for this analysis because it is the shortest band of the three long-wavelength module images, thereby affording the best spatial sampling of the substructures. The PSF model was derived from a median combination of non-saturating stars in the field.

The best-fit model (Figure 3) indicates a primary Sérsic (containing 66% of the total F430M emission) with $n = 0.98$, indicating that the central stellar mass buildup is well-described by an exponential disk; the half-light extent of the disk is 3.3×2.3 kpc with a position angle of 11° (counterclockwise from the north). Subtracting this exponential disk reveals two off-center substructures in the northeast and southwest of the center, which contain 23% and 10% of the total F430M flux, respectively; these three components altogether account for 99% of the total model flux. The northeast substructure (which we will refer to as the ‘northern ridge’ hereafter) is a part

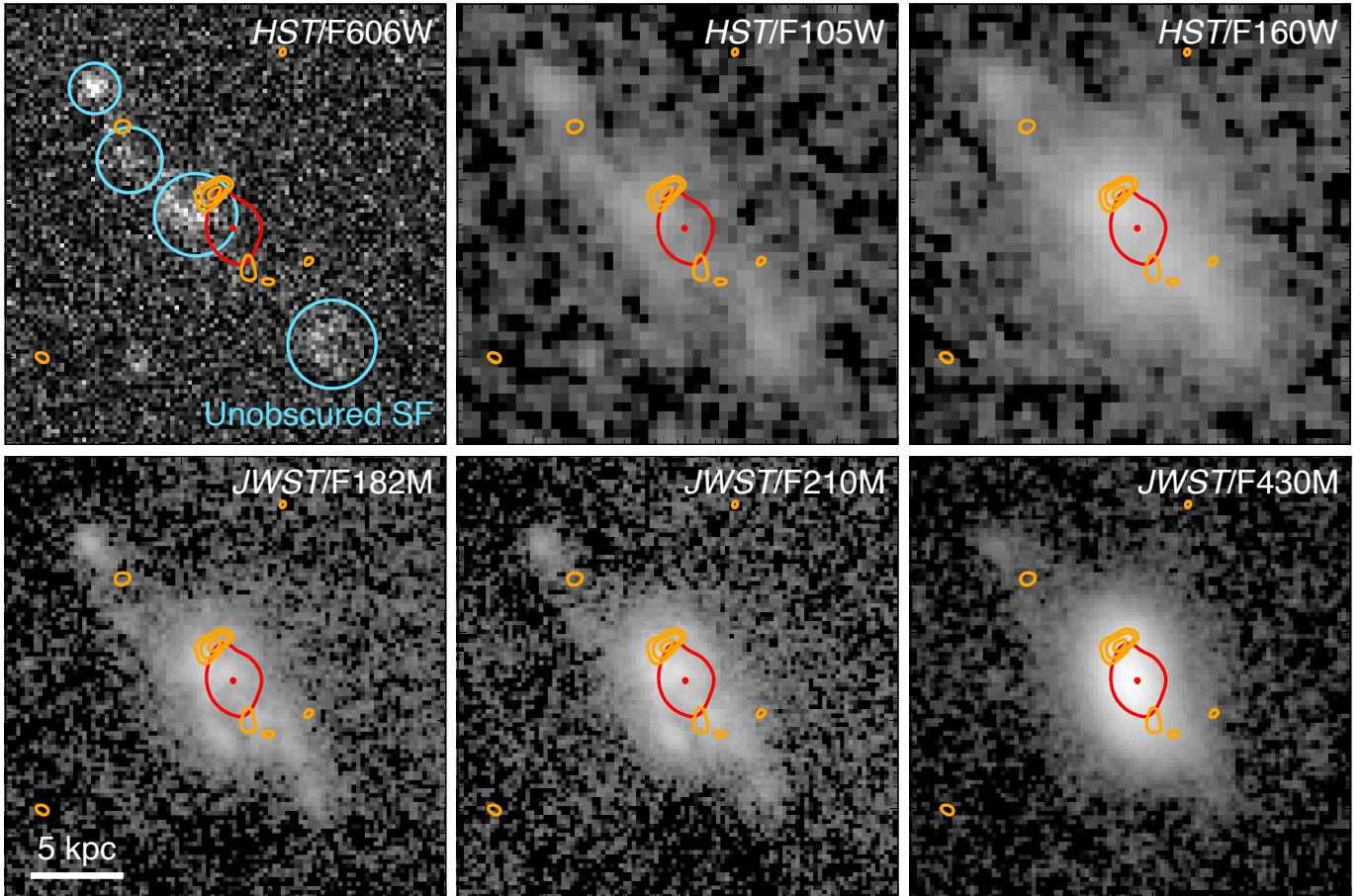


FIG. 4.— The star-forming substructures (orange contours starting from 3σ in 1σ increment), in the context of the rest of the galaxy. Notably, the *HST*/F606W image (rest-frame 160 \AA) shows the spatial dislocation between unobscured SF and the northern ridge; the *JWST*/F182M and F210M images show that the northern ridge appears to be a part of the semicircular arc around the central stellar mass distribution observed at F430M. The red contour delineates the 10σ isophotal extent of unabsorbed ALMA emission (with the red dot marking the peak).

of (and has an elongated shape along) the semicircular feature observed at F210M.

Most significantly, the ALMA substructures are co-located with these F430M substructures, as shown in panel (e) of Figure 3, suggesting that they are off-center stellar mass substructures that harbor ongoing SF. Furthermore, the northern ridge appears to be partially overlapping with point-like features observed at F182M and F210M, which could represent the relatively less dust-attenuated (or patchy) emission from young stars (Figures 3 and 4).

3.4. Physical properties of the off-center substructures

Having established the existence of off-center substructures containing both stellar mass and SF, we put constraints on their physical properties in order to aid the interpretation of their nature. We will focus on the northern ridge in this Letter and follow up with a more comprehensive study of UDF2 in the future when deeper *JWST*/NIRCam and MIRI imaging from the ongoing programs in Cycle 1 becomes available.

The northern ridge, shown in panel (e) of Figure 3, forms an arc spanning the position angle of $\simeq 0 - 50$ deg (counterclockwise from the north) of, and at a distance of $0''.20 - 0''.35$ ($1.6 - 2.8$ kpc) from the center. The length and width of the ridge are $\simeq 2.5 \times 1$ kpc.

The ALMA rest-frame $240 \mu\text{m}$ residual flux in the northern ridge is $\simeq 5\%$ of the total flux. If we assume that dust temperature and IMF do not vary spatially across the galaxy and that SFR varies linearly with the far-IR flux, the inferred SFR within the northern ridge is $\simeq 13 M_{\odot}\text{yr}^{-1}$. We note that the unobscured SFR inferred from rest-frame UV emission is $< 1 M_{\odot}\text{yr}^{-1}$ (Dunlop et al. 2017); its contribution to the SFR of the northern ridge remains small, i.e., even the extended SF in the outer region of the galaxy is strongly dust-obscured. Likewise, the *JWST* rest-frame $1.2 \mu\text{m}$ residual flux in the northern ridge is 23% of the total flux. If we assume a constant IMF and that the stellar mass varies linearly with the $1.2 \mu\text{m}$ flux, the stellar mass in the northern ridge is about $\log(M_*/M_{\odot})$ of 10.2 ± 0.2 . This stellar mass estimate should be taken as an upper limit considering the potential contribution from young stars to the rest-frame $1.2 \mu\text{m}$ emission.

In summary, we have identified, within a typical SFG at $z = 2.7$, two off-center substructures containing $\simeq 10 - 20\%$ of total stellar mass and $\simeq 5\%$ of total SF. We highlight the fact that the central star-forming region is where $\simeq 90\%$ of SF is located and also contains $\simeq 70\%$ of the total stellar mass, which implies that the substructures have $\sim 2 - 4\times$ lower specific SFR (sSFR) compared to that of the center.

4. DISCUSSIONS

There are notable parallels between the substructures identified in this work and those observed at $z \sim 1-4$ using *JWST*. For example, spiral arms have been identified optically by Wu et al. (2023) using NIRCcam observations of A2744-D5G-z3, a typical SFGs at $z = 3.06$, but the angular resolution and sensitivity of their ALMA observations are insufficient to resolve the spiral structures observed by *JWST*. Similarly, using NIRCcam observations of seven sub-mm-selected typical SFGs at $z \sim 2$, Chen et al. (2022) found spiral arms and bars and also nearby companions that suggest ongoing dynamical interactions (their IR/radio observations are \sim few arcsecond resolution, still not sufficient to associate the stellar mass and SF structures). Cheng et al. (2023) observed 19 ALMA-selected cluster-lensed and field galaxies at $z \sim 1-4.5$ spanning both main-sequence and quiescent sSFR ranges using NIRCcam and found substructures such as spiral arms to be common. Their ALMA observations were at $0''.3-2''.1$ angular resolution and start to reveal potential cases of SF within substructures and suggest that definitive associations of SF within off-center stellar-mass substructures could be commonplace with greater availability of high-resolution, high-S/N ALMA observations of NIRCcam targets.

In both the Chen et al. (2022) and Wu et al. (2023) samples, companion and/or group environment appears to be a common attribute. We also find that UDF2 also resides in a potentially overdense region with four massive galaxies (including UDF2) identified within a projected distance of 70 kpc, spectroscopically confirmed (F. Sun, private communication) to be at $z = 2.690-2.697$ (Figure 5). These findings allude to a picture that the stellar-mass substructures with ongoing SF identified in UDF2 could represent a forming spiral arm or other types of disk instability resulting from minor merger or interactions in an overdense environment (despite the overall cold gas velocity field appearing to be kinematically-ordered; Kaasinen et al. 2020).

On the contrary, local spiral arms contain stellar masses $\sim 1-5\%$ of the disk (e.g., Pichardo et al. 2003), significantly smaller than the substructures we have identified. The $2\times$ asymmetry of the stellar mass between the northern and southern ridges of UDF2 is another departure from classical spiral arms and bears a resemblance to the lopsided stellar disk reported by Kalita et al. (2022), who proposed that mass lopsidedness in the stellar disk could be a remnant indicating the ‘impact point’ of the cold gas accretion stream (also in a cluster environment). Another similarity to the Kalita et al. substructure, which is quiescent, is that the northern ridge has $4\times$ lower sSFR compared to the core, and hence could represent an evolutionary stage prior to the Kalita et al. picture. The fueling and highly unstable disk (e.g., a local analog of $z \sim 1-2$ typical SFGs studied in detail by Puschnig et al. 2023) that has led to a structure like that of the northern ridge and the lopsided disks could be characteristic of typical SFGs at $z \sim 3$.

Simulations of gas-rich galactic disks have long predicted the existence of SF clumps, with the latest predictions being that they are $10^7-10^8 M_\odot$ in mass, SFR $\sim 1\%$ of galaxy-integrated SFR, and size $\sim 50-100$ pc (e.g., Mandelker et al. 2017; Tamburello et al. 2017; Faure et al.

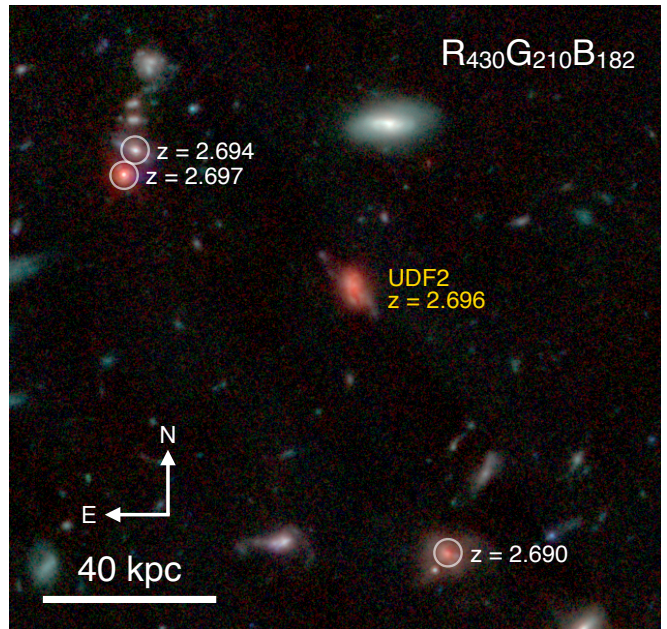


FIG. 5.— Three other massive galaxies spectroscopically confirmed to be at $z = 2.690-2.697$ are within a projected distance of 70 kpc from UDF2, suggesting a potentially overdense region that may have implications on the origin of the substructures identified.

2021; Fensch & Bournaud 2021). So far, the predictions are at odds with the handful of typical SFGs at $z \sim 2-3$ with high-resolution, high-S/N ALMA observations: the central SF regions of UDF2 and other HUDF galaxies are smooth and the strongly-lensed ‘Eyelash’ is also clumpless down to 1% SFR at $\simeq 80$ pc resolution (Rujopakarn et al. 2019; Ivison et al. 2020). It is hence natural to ask if we are finally seeing off-center submm SF clumps here. Perhaps not directly: the northern ridge is significantly larger in stellar mass, SFR, and especially the size than the predicted clumps, though we cannot exclude a scenario that the northern ridge is a structure comprising multiple clumps of SF, which can be tested using higher resolution ALMA observations at higher S/N.

This Letter highlights the importance of the combination of ALMA and *JWST* to probe dusty galactic structure at $z \sim 3$. Apparent voids at shorter wavelengths due to dust obscuration/attenuation are being filled by *JWST*. In the case of UDF2, the location of the bulk of the stellar mass buildup is revealed to be co-located with the starburst core, affording a clearer picture of the galactic bulge during its assembly, and also galactic-disk substructures actively forming stars. Building a statistical sample of disk substructures in typical SFGs with optical/submm counterparts will be crucial to help bridge the gaps between optical/near-IR and far-IR/submm morphologies, as well as between the compact core SF and the rest of the galaxy.

ACKNOWLEDGMENTS

We thank the anonymous referee for their helpful suggestions and comments. This Letter makes use of observations from *JWST* Cycle 1 GO program #1963. Support for program JWST-GO-1963 was provided in part by NASA through a grant from the Space Telescope Science Institute, which is operated by the Associations of Universities for Research in As-

tronomy, Incorporated, under NASA contract NAS 5-26555. The research of CCW is supported by NOIR-Lab, which is managed by the Association of Universities for Research in Astronomy (AURA) under a cooperative agreement with the National Science Foundation. This Letter makes use of the ALMA data from ADS/JAO.ALMA#2017.1.00001.S. ALMA is a partnership of ESO (representing its member states), NSF

(USA) and NINS (Japan), together with NRC (Canada) and NSC and ASIAA (Taiwan) and KASI (Republic of Korea), in cooperation with the Republic of Chile. The Joint ALMA Observatory is operated by ESO, AUI/NRAO and NAOJ. W.R. acknowledges support from Chulalongkorn University's CUniverse and the Ratchadapiseksompot Endowment Fund.

REFERENCES

- Barro, G., Kriek, M., Pérez-González, P. G., et al. 2016, *ApJ*, 827, L32
- Chen, C.-C., Gao, Z.-K., Hsu, Q.-N., et al. 2022, *ApJ*, 939, L7. doi:10.3847/2041-8213/ac98c6
- Cheng, C., Huang, J.-S., Smail, I., et al. 2023, *ApJ*, 942, L19. doi:10.3847/2041-8213/aca9d0
- Cibinel, A., Daddi, E., Bournaud, F., et al. 2017, *MNRAS*, 469, 4683
- Dunlop, J. S., McLure, R. J., Biggs, A. D., et al. 2017, *MNRAS*, 466, 861
- Elbaz, D., Leiton, R., Nagar, N., et al. 2018, *A&A*, 616, A110
- Faure, B., Bournaud, F., Fensch, J., et al. 2021, *MNRAS*, 502, 4641
- Fensch, J. & Bournaud, F. 2021, *MNRAS*, 505, 3579
- Fujimoto, S., Ouchi, M., Kohno, K., et al. 2018, *ApJ*, 861, 7
- Hodge, J. A., Smail, I., Walter, F., et al. 2019, *ApJ*, 876, 130
- Hogg, D. W., & Lang, D. 2013, *PASP*, 125, 719
- Iono, D., Yun, M. S., Aretxaga, I., et al. 2016, *ApJ*, 829, L10
- Ivison, R. J., Richard, J., Biggs, A. D., et al. 2020, *MNRAS*, 495, L1
- Kalita, B. S., Daddi, E., Bournaud, F., et al. 2022, *A&A*, 666, A44
- Kaasinen, M., Walter, F., Novak, M., et al. 2020, *ApJ*, 899, 37
- Nelson, E. J., Tadaki, K.-i., Tacconi, L. J., et al. 2019, *ApJ*, 870, 130
- Mandelker, N., Dekel, A., Ceverino, D., et al. 2017, *MNRAS*, 464, 635
- Pichardo, B., Martos, M., Moreno, E., et al. 2003, *ApJ*, 582, 230
- Puschnig, J., Hayes, M., Agertz, O., et al. 2023, arXiv:2303.13858. doi:10.48550/arXiv.2303.13858
- Rizzo, F., Vegetti, S., Powell, D., et al. 2020, *Nature*, 584, 201
- Rodighiero, G., Daddi, E., Baronchelli, I., et al. 2011, *ApJ*, 739, L40
- Rujopakarn, W., Dunlop, J. S., Rieke, G. H., et al. 2016, *ApJ*, 833, 12
- Rujopakarn, W., Daddi, E., Rieke, G. H., et al. 2019, *ApJ*, 882, 107
- Schreiber, C., Pannella, M., Elbaz, D., et al. 2015, *A&A*, 575, A74
- Simons, R. C., Kassim, S. A., Snyder, G. F., et al. 2019, *ApJ*, 874, 59. doi:10.3847/1538-4357/ab07c9
- Speagle, J. S., Steinhardt, C. L., Capak, P. L., & Silverman, J. D. 2014, *ApJS*, 214, 15
- Spergel, D. N. 2010, *ApJS*, 191, 58
- Swinbank, A. M., Dye, S., Nightingale, J. W., et al. 2015, *ApJ*, 806, L17
- Tadaki, K.-i., Genzel, R., Kodama, T., et al. 2017, *ApJ*, 834, 135
- Tadaki, K., Iono, D., Yun, M. S., et al. 2018, *Nature*, 560, 613
- Tamburello, V., Rahmati, A., Mayer, L., et al. 2017, *MNRAS*, 468, 4792
- Whitaker, K. E., van Dokkum, P. G., Brammer, G., & Franx, M. 2012, *ApJ*, 754, L29
- Williams, C. C., Tacchella, S., Maseda, M. V., et al. 2023, arXiv:2301.09780. doi:10.48550/arXiv.2301.09780
- Wu, Y., Cai, Z., Sun, F., et al. 2023, *ApJ*, 942, L1. doi:10.3847/2041-8213/aca652